Environ. Sci. Technol. **2010,** *44,* 1017–1022

Sources and Pathways of Polycyclic Aromatic Hydrocarbons Transported to Alert, the Canadian High Arctic

RONG WANG,[†] SHU TAO,[†,*] BIN WANG,[†] YU YANG,[†] CHANG LANG,[†] YANXU ZHANG,[†] JING HU,[†] JIANMIN MA,[‡] AND HAYLEY HUNG[‡]

Laboratory for Earth Surface Processes, College of Urban and Environmental Sciences, Peking University, Beijing 100871, China, Air Quality Research Division, Science and Technology Branch, Environment Canada, 4905 Dufferin Street, Toronto, Ontario M3H 5T4, Canada

Received July 26, 2009. Revised manuscript received December 8, 2009. Accepted December 9, 2009.

A probabilistic function (integrated source contribution function, ISCF) based on backward air mass trajectory calculation was developed to track sources and atmospheric pathways of polycyclic aromatic hydrocarbons (PAHs) to the Canadian High Arctic station of Alert. In addition to the movement of air masses, the emission intensities at the sources and the major processes of partition, indirect photolysis, and deposition occurring on the way to the Arctic were incorporated into the ISCF. The predicted temporal trend of PAHs at Alert was validated by measured PAH concentrations throughout 2004. The PAH levels in the summer are orders of magnitude lower than those in the winter and spring when long-range atmospheric transport events occur more frequently. PAHs observed at Alert are mostly from East Asia (including Russia Far East), North Europe (including European Russia), and North America. These sources account for 25, 45, and 27% of PAHs atmospheric level at Alert, respectively. Source regions and transport pathways contributing to the PAHs contamination in the Canadian High Arctic vary seasonally. In the winter, Russia and Europe are the major sources. PAHs from these sources travel eastward and turn to the north at approximately 120°E before reaching Alert, in conjunction with the well-known Arctic haze events. In the spring, PAHs from Russia and Europe first migrate to the west and then turn to the north at 60°W toward Alert. The majority of PAHs in the summer are from northern Canada where they are carried to Alert via low-level transport pathways. In the fall, 70% of PAHs arriving at Alert are delivered from North American sources.

Introduction

Polycyclic aromatic hydrocarbons (PAHs) are among the organic pollutants of greatest public concern, primarily due to their carcinogenic effects (*1*). Although the amount of PAHs released in developed countries has decreased over the past few decades (*2*), the global emission has changed little mainly due to the increase in emissions from developing countries (*3*).

PAHs can migrate to remote pristine areas. Consequently, PAHs emitted at midlatitudes exert a strong influence on PAH abundances in the polar region (*4*). For this reason, PAHs have been listed in the 1998 UNECE (United Nations Economic Commission for Europe) Aarhus Protocol on Persistent Organic Pollutants (POPs) (*5*). With extremely limited local emissions, the Arctic is an ideal region for providing global background values, monitoring the global cycle, and investigating long-range transport and the influence of climate change on the fate of POPs (*6*).

PAHs have been regularly monitored at a number of sites in the Arctic since 1990 (*7*). At Alert, air samples have been collected and analyzed weekly for PAHs and other chemicals for almost two decades as a part of the Canadian Northern Contaminants Program (*8*). The data provides valuable information for better understanding the levels, sources and transport pathways of PAHs over the high Arctic.

Air mass trajectory modeling provides an efficient technique for tracking the movement of atmospheric pollutants. Together with monitored time series of pollutants, the technique has been employed to identify source regions (*8, 9*). It is generally accepted that the major source regions of PAHs observed in the Arctic are from Eurasia. For example, during severe contamination events, the observed PAHs at Alert were traced back to Norilsk, northern Siberia, and the Kola Peninsula of western Siberia (*8*). One high-level and two low-level atmospheric pathways have been identified through which black carbon is transported from the major source region of Europe to the Arctic (*10*). Even South Asia can be an important source region for black carbon levels in the Arctic (*11*).

Whereas simple trajectory calculation can only provide information on transport routes and major source locations of pollutants, the statistical model based on trajectory calculation may help to quantify the atmospheric transport to a certain extent. Typical examples of probabilistic models include a potential source contribution function, a non-parametric regression model, and a source-region impact factor (*12–14*). Lately, Lang et al. attempted to incorporate emission and decay processes in a forward trajectory model and to quantitatively characterize the outflow of PAHs from China (*15*).

This study makes a further effort to 1) develop a probabilistic model, based on backward air mass trajectory calculations with major removal processes included, for investigating the source−receptor relationship, and 2) investigate the sources and pathways of PAHs observed at Alert in the Arctic as well as their seasonality. An integrated source contribution function (ISCF) was developed to predict the contributions of various source regions. Major processes were source emission and removal processes in the atmosphere, including partition, indirect photolysis as an OH radical reaction, and depositions. The modeled 15 PAHs include acenaphthylene (ACY), acenaphthene (ACE), fluorene (FLO), phenanthrene (PHE), anthracene (ANT), fluoranthene (FLA), pyrene (PYR), benz[a]anthracene (BaA), chrysene (CHR), benzo[b]fluoranthene (BbF), benzo[k]fluoranthene (BkF), benzo[a]pyrene (BaP), dibenz[a,h]anthracene (DahA), indeno[l,2,3-cd]pyrene (IcdP), and benzo[g,h,i]perylene (BghiP).

Materials and Methods

Study Site and Air Sampling. Located in northern Ellesmere Island, Nunavut (82°30′N, 62°20′W), Alert is the master air monitoring station operated by the Canadian Northern Contaminants Program. Routine air monitoring for persistent organic pollutants at Alert has been conducted since 1992.

* Corresponding author phone and fax: 0086-10-62751938; e-mail: taos@urban.pku.edu.cn.
[†] Peking University.
[‡] Environment Canada.

10.1021/es902203w
Published on Web 12/29/2009

Weekly air samples are collected with a superhigh-volume air sampler mounted on a 10 m high sampling tower at the Alert Global Atmospheric Watch Station. One glass fiber filter and two polyurethane foam plugs are used in each sample to trap the respective particle and gas-phase chemicals in ~13 000 m^3 of air over 7 days. Sampling details, sample preparation, analysis, and data quality control/assurance protocols are referred to a previous publication (*16*).

Backward Air Mass Trajectories. Backward air mass trajectories were calculated using the NOAA hybrid single-particle Lagrangian integrated trajectory model, driven by meteorological variables collected from global NOAA-NCEP/NCAR pressure level reanalysis data (*17*). The trajectories for 20 days were calculated to enable major source regions to be covered properly. Given the relatively large errors at near ground levels in trajectory calculations (*12*), a set of 10 trajectories was calculated at 10 starting points from 100 to 1000 m at 100 m intervals above ground at Alert. The model was integrated for the period from December 27, 2003 to January 5, 2005 using six-hourly meteorological data at 0:00, 6:00, 12:00, and 18:00 h (UTC). The coordinates of the calculated trajectory points (vertically up to 10 km) were recorded at 1 h time intervals.

Global Emission Inventory. A country-level global emission inventory of PAHs was used in the present study (*3*). It was further updated by replacing the emission factors of aluminum electrolysis and petroleum fuel for high-income countries using the lately published data (*18, 19*). The emission within each country was interpolated into a 1° × 1° resolution based on its population for 2004 (*20*) under the assumption that the emission was population density dependent (*21*). A high spatial resolution inventory for China was used directly (*21*). Seasonal variation in the emission was characterized by estimating the monthly average emission based on a relationship between fuel consumption and ambient air temperature (*22*). The emission inventory for the total of the 15 PAHs is mapped in section S1 of the Supporting Information.

Integrated Source Contribution Function. Preliminary trajectory analysis showed that trajectories initiated from the near ground level (e.g., 5 m, 10 m, 20 m above ground) at Alert appeared not extended beyond the Arctic. From this fact, we defined an integrated source contribution function (ISCF) (pg/m^3) as the mean concentration of a given PAH averaged over the 10 vertical levels at Alert (eq 1). The concentration at each height (starting point of a trajectory) was the sum of contributions from various source grids through which the trajectory passed (the value was zero if no trajectory passed through). The target region was the globe and the horizontal resolution was 1° × 1°.

$$\mathrm{ISCF} = \frac{1}{10}\sum_{h=1}^{10}\sum_{x=1}^{180}\sum_{y=1}^{360}\mathrm{ISCF}_{hxy} \quad (1)$$

ISCF_{hxy} (pg/m^3) represents the total contribution from a grid (x,y) to the h^{th} starting point, and x and y are the x^{th} and y^{th} meridian and zonal grid respectively. ISCF_{hxy} is calculated as the sum of contributions of each hour for the trajectory staying in the grid (eq 2).

$$\mathrm{ISCF}_{hxy} = s\sum_{t=i}^{i+j}(L_{hxyt}M_{hxyt}),\ x = 1...180,\ y = 1...360,\ h = 1...10 \quad (2)$$

t (hour) is trajectory time. i represents the time at which the trajectory entered the given grid (x, y) and j (hour) is the duration of the trajectory staying at the grid, respectively. s is the time step of the calculation, set at 1 h in this study. M_{hxyt} is the remaining fraction of the given PAH in the air parcel due to the removal processes during the transport from the grid (x, y) to the h^{th} starting point at Alert, whereas L_{hxyt} (pg/m^3·hour) represents the loading of the given PAH at the grid (x, y) into the trajectory at time t. L_{hxyt} is calculated as a height-weighted function of the emission and atmospheric boundary layer height (eq 3).

$$L_{hxyt} = \frac{V_b}{\sum_{b=1}^{10}V_b}\frac{E_{hxyt}}{H_{hxyt}},\ x = 1...180,\ y = 1...360,\ h = 1...10,\ t = i...i+j \quad (3)$$

E_{hxyt} (pg/m^2·hour) and H_{hxyt} (m) are the emission flux and the atmospheric boundary layer height at the grid (x, y) at time t. The source grid was divided into 10 layers at equal intervals within the atmospheric boundary height and V_b is a weighting factor for the b^{th} layer to scale the relative contribution of the ground-level PAH emission to air concentrations in that layer. The lower level in the atmospheric boundary layer tends to receive a higher contribution from the ground emission under the dominant stable condition (e.g., downward flux > turbulent transfer), which is always reported in source regions (*23*). Extensive numerical analyses to the model results showed that the effect of the emission within the atmospheric boundary layer was negatively correlated with altitude ($V_b = {}^1/_b$). Contribution was not loaded from the ground emission when the trajectory was above the atmospheric boundary layer.

The remaining fraction (M_{hxyt}) due to removal processes during the transport from the grid (x, y) to the h^{th} height at Alert is calculated using eq 4 where M_{hxyt} is simplified as M_t.

$$M_t = R_{t\tau}|_{\tau=t} \quad (4)$$

$R_{t\tau}$ represents the remaining fraction of PAH after τ hours' transport in the air parcel starting from the grid (x, y). With a first-order kinetic assumption for the removal processes, $R_{t\tau}$ can be written as eq 6.

$$R_{t\tau} = R_{t\tau-1}e^{-K_{\tau-1}s} = e^{-s(K_0+K_1+...+K_{\tau-1})},\ \tau = 1, 2, ...t \quad (5)$$

s (hour) is the time step (1 h). $K_{\tau-1}$ (1/hour) is the decay constant during a period from $\tau - 1$ to τ. As indicated by Halsall et al. (*4*), the decay constant can be calculated based on the partition between the gaseous and particulate phases, indirect photolysis, and wet and dry depositions, given by eqs 6 and 7.

$$\frac{\mathrm{d}R_{t\tau}}{\mathrm{d}\tau} = -f_P R_{t\tau}\cdot\frac{v_d}{W} - (1 - f_P)\cdot R_{t\tau}\cdot K_{OH}\cdot[OH] - R_{t\tau}\cdot\frac{S_c\cdot I}{H} = -K_\tau \times R_{t\tau} \quad (6)$$

$$K_\tau = f_{\mathrm{P}}\frac{v_{\mathrm{d}}}{W} + (1 - f_{\mathrm{P}})K_{\mathrm{OH}}[\mathrm{OH}] + \frac{S_{\mathrm{c}}I}{H} \quad (7)$$

f_{P} is the fraction of particulate phase PAH. v_{d} (m/h) is the stability-dependent dry deposition velocity and W (m) is the thickness of the layer (200 m), defined by Pistocchi (*24*) and used by Lang et al. (*15*). The settling velocity was not considered due to its relative small magnitude as compared to v_{d} (*4, 15*). S_{c} is the total wet deposition scavenging coefficient. H (m) is the thickness of the atmospheric boundary layer. [OH] (molecules/cm^3) and K_{OH} (cm^3/molecules·s) are OH radical concentration and reaction rate constant of PAH with OH radicals, respectively. I (mm/h) is precipitation rate. Molecular diffusion was not included because it is significantly slower than dry deposition (high molecular weight PAHs) or indirect photolysis (low molecular weight PAHs) (*25*). [OH] was derived from monthly archived

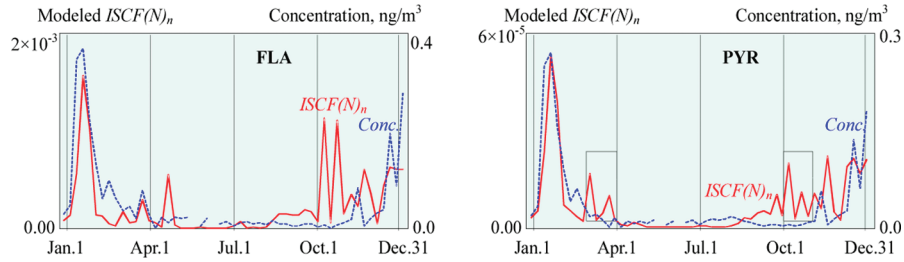

FIGURE 1. Comparison in the time series of FLA and PYR between the model-predicted ISCF(N)$_n$ and the field-observed concentrations at Alert in 2004.

global data (GEOS-CHEM, 2° × 2.5° horizontally) (*26*) because daily data was not available. The modeling procedure is graphically presented in section S2 of the Supporting Information. Detailed information for derivation of f_p, υ_d, S_c, H, K_{OH} and other parameters used in the model is summarized in section S3 of the Supporting Information.

Normalization of Integrated Source Contribution Function. It should be pointed out that the model has a number of intrinsic limitations. First, a number of processes and factors, such as gaseous diffusion between air and surface, particle size distribution, and diurnal variation in OH concentration were not taken into consideration; second, some parameters (e.g., precipitation rate and OH concentrations) were subject to some uncertainties; and third, relatively high uncertainties in the 20 day trajectory calculations were expected. Therefore, the final results are presented as probabilities rather than concentrations. Although air concentrations cannot be derived, their temporal trends and spatial patterns can be well represented by the ISCFs as presented below.

The probabilistic functions were derived by normalizing ISCF or ISCF$_{xy}$ for a certain period of time. ISCF was averaged for a number of trajectory sets (e.g., daily average of 4 sets, weekly average of 28 sets). As shown in eq 8, the averaged functions were then normalized for a given period of time with N averaged ISCF values.

$$\mathrm{ISCF}(N)_n = \frac{\mathrm{ISCF}_n}{\sum_{k=1}^{N} \mathrm{ISCF}_k},\ n = 1...N \tag{8}$$

ISCF$_k$ is the averaged *ISCF* for the k^{th} trajectory set. A total of N ISCF$(N)_n$ values predict the time series of the pollution level at Alert. For example, to compare with the weekly measured PAH concentrations, 53 weekly mean ISCFs were normalized, where ISCF$_k$ was the averaged ISCF for an individual week (N = 53). On the other hand, ISCF$_{xy}$ values for a given period of time were normalized for all trajectories as eq 9.

$$\mathrm{ISCF}(N)_{xy} = \frac{\sum_{k=1}^{N}\left(\frac{1}{10}\sum_{h=1}^{10}\mathrm{ISCF}_{hxyk}\right)}{\sum_{k=1}^{N} ISCF_k},\ x = 1...180,\ y = 1...360 \tag{9}$$

ISCF$_{hxyk}$ is the ISCF$_{hxy}$ in the k^{th} trajectory. For example, in this study, weekly mean ISCF$(N)_{xy}$ was to be employed to analyze the weekly source distributions, a total of 7 × 4 trajectories (N = 28) were normalized to draw out the contributions from individual grids. The values of ISCF$(N)_{xy}$ calculated at all grids in the globe for the given period of time depict the time-averaged spatial distribution of source contributions to PAH contamination at Alert. In this study, ISCF$(N)_n$ and ISCF$(N)_{xy}$ were used for individual PAH and an average ISCF$(N)_{xy}$ for the 15 PAHs was noted as PAH15. As ISCF$(N)_{xy}$ has been normalized for each PAH before averaging, the sum of ISCF$(N)_{xy}$ of PAH15 for all grids in the globe also equals to the unity.

Model Validation. Weekly averaged measurements for air concentrations of PAHs at Alert for the period from 2003/12/29 to 2005/1/5 were obtained as the sum of the gaseous and particulate phases. The temporal trends were compared with the annually normalized ISCF$(N)_n$ values based on weekly averaged ISCF for model validation.

Results and Discussion

Time Series of PAHs at Alert. The annually normalized ISCF$(N)_n$ based on weekly averaged ISCFs are compared with the measured weekly average PAH concentrations at Alert for 2004. Results are shown in Figure 1. FLA and PYR, the only two compounds with all measured concentrations above the detection limits, are presented in the figure. The model-predicted temporal patterns of ISCF$(N)_n$ match generally well with those from the field observations, showing lower levels of PAHs from April to September and higher and fluctuating values during the other months. The two most severe pollution episodes occurring in late January (2004/1/12−2004/2/2) and late December (2004/12/13−2005/1/3) were predicted by the model. The peak concentrations of FLA and PYR were found in January at 253 pg/m^3 and 171 pg/m^3 respectively, and December at 153 pg/m^3 and 98 pg/m^3, respectively. These values are a factor of 3−5 higher than the annual means. Both pollution events featured by poleward atmospheric transport under the Siberia high pressure and the Icelandic low, which forms the poleward atmospheric pathways from Siberia to the high Arctic. In addition, the high PAH emission rate in northern Eurasian countries due to winter heating provides strong sources (*8*).

However, the model results do not match all of the fluctuations of the air concentrations, like March and October. The error of the model is expected to increase when the vertical exchange is weak because ISCF$(N)_n$ is calculated over the 100−1000 m above the ground, whereas the observation is taken near the ground surface (10 m). In fact, the descending motion over the high Arctic happens to be the weakest in March and October during the year (section S4 of the Supporting Information). March and October are transition months from winter to summer and summer to winter during which warmer air mass from midlatitudes is readily penetrated to the Arctic, thereby weakening the polar high pressure and more frequent ascending motions would take place (*27*). Stohl et al. also indicate that the vertical movement of air mass cannot be well predicted by the trajectory calculation (*28*). The limitations of the present model as described in the methodology are also the possible reasons, especially for the fact that daily OH radical concentration data is unavailable. In addition to the two PAHs, there are 11 compounds with the measured winter concentrations above the detection limits. The comparisons between measured and modeled levels for these 11 compounds are illustrated in section S5 of the Supporting Information. Major

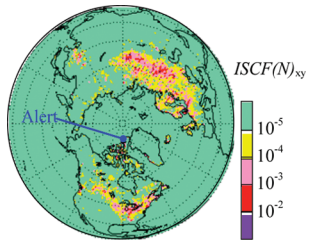

FIGURE 2. Geographical distributions of annual mean ISCF(N)$_{xy}$ values of PAH15 representing the global distributions of source regions of PAHs observed at Alert.

pollution occurrences and temporal trends are well modeled for most of them.

Sources of PAHs. The annual mean ISCF(N)$_{xy}$ distributions for PAH15 are illustrated in Figure 2, showing the major source regions for Alert. Similar results are shown for FLO, PYR, and BaP as representative compounds for low, middle, and high molecular weight PAHs respectively in section S6 of the Supporting Information. The relative contribution of a given source region can be quantified by summing ISCF$_{xy}$ of all cells within this region. It is found that almost all PAHs at Alert were from the northern hemisphere. The three major source regions are North Europe (including European Russian), North America, and East Asia (including Russia Far East), which contribute to 45, 27, and 25% of the total, respectively. As a minor source, northeast China accounts for only 2% of the total. Similar findings on source distributions of air pollutants reaching the Arctic has been reported previously (*10, 11*). The relative contributions of various source regions are different among the compounds. For example, Russia and Canada contribute to 62% and 7% of FLO and 48% and 16% of PYR, respectively. Such a difference is likely due to the difference in emission compositions from various source regions as well as the difference in the long-range transport potentials of various compounds (*4*).

If a given emission activity, rather than all emissions, is used for calculating ISCF, the derived results represent the contribution of the given activity to those that reached Alert. By calculating ISCF values for all individual sources, the relative contributions of major emission activities are derived and listed in section S6 of the Supporting Information for PAH15 and the three representative PAHs (FLO, PYR, and BaP). The most important emission activities are biofuel combustion (24%), followed by aluminum electrolysis (22%), and domestic coal burning (21%). Because of the difference in the source distribution among the major source regions and the difference in the long-range transport potentials of various compounds, the relative contributions of various sources to PAHs contaminations at Alert are different among PAH compounds. For example, 24% of FLO and 16% of PYR are from biofuel burning, whereas aluminum production contributes to 22% of FLO and 26% of PYR.

Seasonality of the Source Contributions. As presented in Figure 1, atmospheric PAHs at Alert vary dramatically for different seasons. The average total concentrations of the 15 PAHs in the winter (1130 ± 741 ng/m^3) are 1 order of magnitude higher than those in the spring (194 ± 142 ng/m^3), fall (137 ± 175 ng/m^3), and summer (82 ± 39 ng/m^3). It is suggested that such seasonality can be attributed to weaker transport potential in the warm season (*8*). From a meteorological perspective, atmospheric long waves break down to shorter waves in the summertime, making long-range transport seldom (*29*). When seasonal variation in PAH emission in the major source regions was quantified, it is evident that relatively higher emission in the winter is another important reason for heavier pollution during this time. Such seasonality in the emission is also documented in the literature. For example, PHE emitted from nonpoint sources

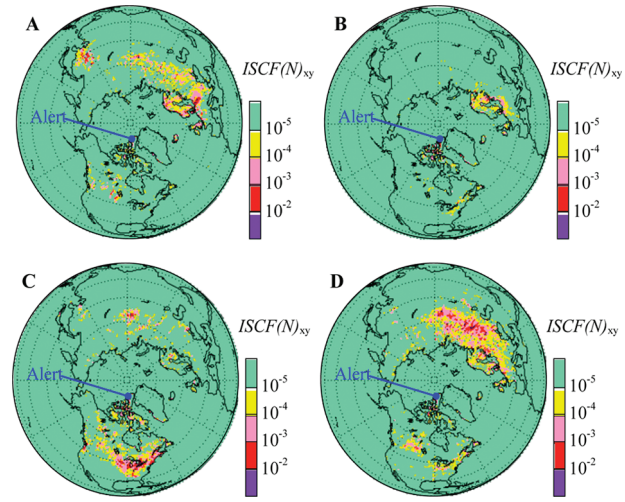

FIGURE 3. Geographical distributions of seasonal mean ISCF(N)$_{xy}$ values of PAH15 representing the global distributions of source regions of PAHs observed at Alert in the four seasons. A, spring; B, summer; C, fall; D, winter.

in North America in a winter day (January 8) is orders of magnitude higher than that in a summer day (July 9) (*30*), which is in agreement with that predicted by the fuel consumptions−temperature relationship used in this model (*22*). The seasonal variation is also apparent in the geographical distribution of the major source regions, as shown in Figure 3 for the averaging of ISCF(N)$_{xy}$ of PAH15 in the spring (March to May), the summer (June to August), the fall (September to November), and the winter (December to February). Although seasonal trends of various PAH compounds agree with one another in general, some differences can still be found (section S7 of the Supporting Information). Detailed results on the seasonality of contributions of various source sectors and regions are also listed in section S8 of the Supporting Information.

In the cold seasons of the northern hemisphere, air masses move predominantly from Eurasia to the high Arctic under the strong influence of the Siberian high and the Icelandic low (*31*). This strong air flow retards the input of pollutants from North America (*27*). Consequentially, Russia and European countries become the major source regions of air pollutants in the spring and winter − the so-called Arctic haze (*31*). This study reveals that Russia and European countries also contribute to 56% and 85% of the total PAHs measurable at atmospheric levels at Alert in spring and winter, respectively. Koch et al. find a similar phenomenon for black carbon and they suggest that almost half of the black carbon observed in the Arctic lower troposphere from January to March is attributable to Russia and Europe emissions, whereas 20% is from North America (*11*). They also indicate that 20% of the black carbon reaching the Arctic is from South Asia (*11*). The relatively low contribution of South Asian sources to PAHs (0.3% in the winter and 14% in the spring, respectively) at Alert is likely caused by the shorter half-life of PAHs in air (1−4 days) than that of black carbon (6 ± 2 days) (*4, 10*). Another possible reason is that strong Siberia High during the wintertime retards south to north transport of PAHs from their Asian source regions (*31*).

The atmospheric transport of PAHs from Eurasian to the Canadian Arctic is weakened in the summer when the air masses reaching Alert are largely from North Pacific and North Atlantic oceans (*10*). Together with low emission rates and fast removal rate under high OH radical concentration and high temperature, the input of PAHs to the Arctic from remote regions diminishes. The major source regions, mainly from biomass burning, are narrowed to the Nunavut Territory of Canada and Greenland, which contribute to over 90% of the

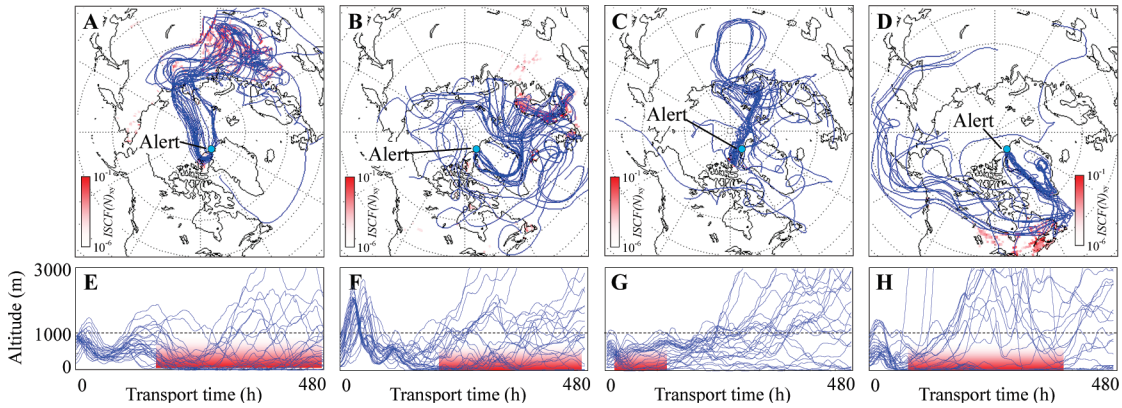

FIGURE 4. Top: Top-view of the 20 day trajectories of the 10% most severely polluted air masses during the most heavily polluted weeks for winter (A), spring (B), summer (C), fall (D). The distributions of the major source regions are shown in red in the background as the weekly mean ISCF(M)$_{xy}$ for PYR. Bottom: side view of the trajectories showing the vertical movement for winter (E), spring (F), summer (G), fall (H). The major source regions are also shown in red.

total atmospheric level of PAHs at Alert. Forest fire in northern Canada is likely a source of PAHs at Alert (*32*). In the fall, North America, particularly the eastern United States, becomes the major source region contributing to 70% of the total PAHs to their level at Alert, whereas the contribution from the Euro-Asian continent drops to 18%.

Pathways of PAH Transported from the Source Regions to Alert. In addition to providing the source information, the calculated trajectories also convey the message on the transport pathways of PAHs from their source regions to Alert. To illustrate the major pathways of long-range transport of PAHs to Alert, the most severely polluted week (with the highest weekly mean ISCF(N)$_n$ for PYR) for each season was selected (January 19−25, April 19−25, July 19−25, and October 4−10 for the four seasons, respectively). Of the 280 trajectories calculated for each week, the top 10% (28 trajectories), which contribute the most to ISCF(N) for PYR, are shown in Figure 4. These trajectories account for more than 99% of PYR transported from their sources to Alert in the selected weeks. Both top and side views of the 20 day trajectories are shown in the figure. The pathway varies seasonally. In the winter, air-laded PAHs in the major source regions of Europe and West Russia, moved eastward, and then turned to the north at approximately 120°E, passing over Siberia all the way to the Arctic and finally reached Alert. In the spring, PAHs emitted from Europe as the major source region traveled to the west first, then turned to the north at 60°W and passed over Greenland, and finally reached Alert. Although there was a small fraction of PAHs from Europe traveling directly northward to Alert, the summer was the only season when local input from islands in northern Canada become more important. A fraction of PAHs reaching Alert was from low-level transport pathways during this season (*10*). A totally different pattern was observed in the fall when North America became the major source region. PAHs were carried by the midlatitude westerly from west to east across the North American continent and turned to the north at 50°W before reaching Alert.

PAHs in the air are almost exclusively from ground sources and their concentrations usually decline with the increase in height (*23*). PAHs can hardly travel to remote areas in the lower troposphere where they move slowly due to the surface friction, deposit easily, and disperse fast under high temperature and strong turbulent activities (*33*). For all four seasons, and especially the spring, fall, and winter, the air parcels laded PAHs by passing the major source regions at low altitudes. For most of those PAHs that finally reach Alert, they are carried to a higher altitude, travel to the Arctic at the midtroposphere, and sink in the high Arctic. Such an atmospheric transport pattern has been often reported (*34*).

Acknowledgments

The field-observed data on time series of PAHs in ambient air were collected and financially supported by the Northern Contaminants Program (Indian and Northern Affairs, Canada) and were kindly provided by Dr. Yushan Su. Funding of this study was provided by the National Science Foundation of China (Grants 140710019001 and 40730737) and National Basic Research Program (2007CB407301).

Supporting Information Available

Detailed information on emission inventory, model calculation and parametrization, descending motion, model validation, source distribution, sector and regional contributions, and seasonality in source geographic distributions. This material is available free of charge via the Internet at http://pubs.acs.org.

Literature Cited

(1) Boffetta, P.; Jourenkova, N.; Gustavsson, P. Cancer risk from occupational and environmental exposure to polycyclic aromatic hydrocarbons. *Cancer Causes & Control* **1997**, *8*, 444–472.
(2) World Health Organization. *Air Quality Guidelines for Europe*, 2nd edition; WHO Regional Office for Europe: Geneva, 2000.
(3) Zhang, Y. X.; Tao, S. Global atmospheric emission inventory of polycyclic aromatic hydrocarbons (PAHs) for 2004. *Atmos. Environ.* **2009**, *43*, 812–819.
(4) Halsall, C. J.; Sweetman, A. J.; Barrie, L. A.; Jones, K. C. Modeling the behavior of PAHs during atmospheric transport from the UK to the Arctic. *Atmos. Environ.* **2001**, *35*, 255–267.
(5) UNECE: Convention on Long-Range Transboundary Air Pollution (LRTAP) on Persistent Organic Pollutants (POPs). Available at http://www.unece.org/env/lrtap.
(6) Law, K. S.; Stohl, A. Arctic air pollution: Origins and impacts. *Science* **2007**, *315*, 1537–1540.
(7) Hung, H.; Halsall, C. J.; Blanchard, P.; Li, H. H.; Fellin, P.; Stern, G.; Rosenberg, B. Temporal trends of organochlorine pesticides in the Canadian Arctic atmosphere. *Environ. Sci. Technol.* **2002**, *36*, 862–868.
(8) Halsall, C. J.; Barrie, L. A.; Fellin, P.; Muir, D. C. G.; Billeck, B. N.; Lockhart, L.; Rovinsky, F. Y.; Kononov, E. Y.; Pastukhov, B. Spatial and temporal variation of polycyclic aromatic hydrocarbons in the Arctic atmosphere. *Environ. Sci. Technol.* **1997**, *31*, 3593–3599.
(9) Helm, P. A.; Bidleman, T. F.; Li, H. H.; Fellin, P. Seasonal and spatial variation of polychlorinated naphthalenes and non-/mono-ortho-substituted polychlorinated biphenyls in Arctic air. *Environ. Sci. Technol.* **2004**, *38*, 5514–5521.
(10) Stohl, A. Characteristics of atmospheric transport into the Arctic troposphere. *J. Geophys. Res., [Atmos.]* **2006**, *111*, (D11).

(11) Koch, D.; Hansen, J. Distant origins of Arctic black carbon: A Goddard Institute for Space Studies Model experiment. *J. Geophys. Res., [Atmos.]* **2005**, *110*, (D4).
(12) Stohl, A. Trajectory statistics - A new method to establish source-receptor relationships of air pollutants and its application to the transport of particulate sulfate in Europe. *Atmos. Environ.* **1996**, *30*, 579–587.
(13) Hoh, E.; Hites, R. A. Sources of toxaphene and other organochlorine pesticides in North America as determined by air measurements and potential source contribution function analyses. *Environ. Sci. Technol.* **2004**, *38*, 4187–4194.
(14) Primbs, T.; Simonich, S.; Schmedding, D.; Wilson, G.; Jaffe, D.; Takami, A.; Kato, S.; Hatakeyama, S.; Kajii, Y. Atmospheric outflow of anthropogenic semivolatile organic compounds from East Asia in spring 2004. *Environ. Sci. Technol.* **2007**, *41*, 3551–3558.
(15) Lang, C.; Tao, S.; Zhang, G.; Fu, J.; Simonich, S. Outflow of polycyclic aromatic hydrocarbons from Guangdong, Southern China. *Environ. Sci. Technol.* **2007**, *41*, 8370–8375.
(16) Fellin, P.; Barrie, L. A.; Dougherty, D.; Toom, D.; Muir, D.; Grift, N.; Lockhart, L.; Billeck, B. Air monitoring in the Arctic: Results for selected persistent organic pollutants for 1992. *Environ. Toxicol. Chem.* **1996**, *15*, 253–261.
(17) Draxler, R. R.; Rolph, G. D. HYSPLIT (Hybrid Single-Particle Langrangian Integrated Trajectory) Model; 2003.
(18) 2000 Criteria Air Contaminant Emission Inventory; Environment Canada, 2004.
(19) Ketzel, M.; Wahlin, P.; Berkowicz, R.; Palmgren, F. Particle and trace gas emission factors under urban driving conditions in Copenhagen based on street and roof-level observations. *Atmos. Environ.* **2003**, *37*, 2735–2749.
(20) LandScan Global Population 2004 Database; Oak Ridge National Laboratory (ORNL), 2005.
(21) Zhang, Y. X.; Tao, S.; Cao, J.; Coveney, R. M. Emission of polycyclic aromatic hydrocarbons in China by county. *Environ. Sci. Technol.* **2007**, *41*, 683–687.
(22) Zhang, Y. X.; Tao, S. Seasonal variation of polycyclic aromatic hydrocarbons (PAHs) emissions in China. *Environ. Pollut.* **2008**, *156*, 657–663.
(23) Tao, S.; Wang, Y.; Wu, S. P.; Liu, S. Z.; Dou, H.; Lu, Y. N.; Lang, C.; Hu, F.; Xing, B. S. Vertical distribution of polycyclic aromatic hydrocarbons in atmospheric boundary layer of Beijing in winter. *Atmos. Environ.* **2007**, *41*, 9594–9602.
(24) Pistocchi, A. A GIS-based approach for modeling the fate and transport of pollutants in Europe. *Environ. Sci. Technol.* **2008**, *42*, 3640–3647.
(25) Gardner, B.; Hewitt, C. N.; Jones, K. C.; Smith, D. Deposition of PAHs to natural water surfaces in the UK. In *Precipitation Scavenging and Atmosphere Exchange*; Schwatz, S. E., Slinn, W. G. N., Eds.; Hemisphere Pub. Corp: Washington, D.C., 1993; Vol. 2.
(26) Harvard University GEOS-Chem program: GEOS-CHEM monthly archived global data (2 × 2.5 degree resolution). Available at http://acmg.seas.harvard.edu/geos/geos_hi_res.html.
(27) Klonecki, A.; Hess, P.; Emmons, L.; Smith, L.; Orlando, J.; Blake, D. Seasonal changes in the transport of pollutants into the Arctic troposphere-model study. *J. Geophys. Res., [Atmos.]* **2003**, *108*, (D4).
(28) Stohl, A.; Hittenberger, M.; Wotawa, G. Validation of the Lagrangian particle dispersion model FLEXPART against large-scale tracer experiment data. *Atmos. Environ.* **1998**, *32*, 4245–4264.
(29) Georgieva, K.; Kirov, B.; Tonev, P.; Guineva, V.; Atanasov, D. Long-term variations in the correlation between NAO and solar activity: The importance of north-south solar activity asymmetry for atmospheric circulation. *Adv. Space Res.* **2007**, *40*, 1152–1166.
(30) Galarneau, E.; Makar, P. A.; Sassi, M.; Diamond, M. L. Estimation of atmospheric emissions of six semivolatile polycyclic aromatic hydrocarbons in southern Canada and the United States by use of an emissions processing system. *Environ. Sci. Technol.* **2007**, *41*, 4205–4213.
(31) MacDonald, R. W.; Barrie, L. A.; Bidleman, T. F.; Diamond, M. L.; Gregor, D. J.; Semkin, R. G.; Strachan, W. M. J.; Li, Y. F.; Wania, F.; Alaee, M.; et al. Contaminants in the Canadian Arctic: 5 years of progress in understanding sources, occurrence and pathways. *Sci. Total Environ.* **2000**, *254*, 93–234.
(32) Fu, P. Q.; Kawamura, K.; Barrie, L. A. Photochemical and other sources of organic compounds in the Canadian high arctic aerosol pollution during winter-spring. *Environ. Sci. Technol.* **2009**, *43*, 286–292.
(33) Zhang, L. S.; Ma, J. M.; Venkatesh, S.; Li, Y. F.; Cheung, P. Modeling evidence of episodic intercontinental long-range transport of lindane. *Environ. Sci. Technol.* **2008**, *42*, 8791–8797.
(34) Liang, Q.; Jaegle, L.; Jaffe, D. A.; Weiss-Penzias, P.; Heckman, A.; Snow, J. A. Long-range transport of Asian pollution to the northeast Pacific: Seasonal variations and transport pathways of carbon monoxide. *J. Geophys. Res., [Atmos.]* **2004**, *109*, (D23).

ES902203W